WaveComBE

mmWave Communications in the Built Environments

WaveComBE_D1.3

Massive MIMO antenna prototypes

Version v1.0 Date: 2021/04/01

Document properties:

Grant Number:	766231
Document Number:	D1.3
Document Title:	Massive MIMO antenna prototypes
Partners involved:	University of Twente, Gapwaves
Authors:	Alireza Bagheri Moghim, Wai Yan Yong, Carlo Bencivenni, Abolfazl Haddadi, Hanna Karlsson, Magnus Gustafsson, Thomas Emanuelson, Marcus Hasselblad, Andrés Alayón Glazunov
Contractual Date of Delivery:	2021/04/01
Dissemination level:	CO[1]
Version:	1.0
File Name:	WaveComBE D1.3_v1.0

[1] CO = Confidential, only members of the consortium (including the Commission Services)

[2] PU = Public

Table of contents

Table of contents 3
Executive Summary 4
List of figures 5
List of Acronyms and Abbreviations 6
1. Introduction 7
2. A 28-GHz 8x8 phased array antenna based on Gap waveguide with 60dBm EIRP 8
2.1 Antenna structure description 8
2.2 Passive measurements 8
2.2.1 Setup calibration with standard horn antenna 8
2.2.2 Measuring loss in the passive board 9
2.2.3 Computing the antenna based on the passive measurement setup 10
2.3 Active Measurements 11
2.3.1 Measuring gain of the active board 11
2.3.2 Computing the radiation gain pattern at different tilting angles 12
3. A 28-GHz 16x16 phased array based on Gap waveguide with 45°-slanted polarization and 65dBm EIRP. 16
3.1 Phased Array Design 16
3.1 Antenna Design and Measurements 18
3.2 Calibration and Pattern Measurement of the PAAM 19
4. Conclusions 20
A. List of Publications (published and in preparation) 21
References 22

Executive Summary

The development of advanced antenna technologies and designs is at the core of 5G communications systems. In this report, we present numerical designs phased array antenna designs at the mmWave (millimeter wave) frequencies. Both phased arrays antennas have been manufactured and characterized. The first is a 28-GHz 8x8 phased array with 60dBm EIRP. The second is a 28-GHz 16x16 phased array with 45°-slanted polarization and 64 dBm EIRP. The 45°-slant polarization reduces the manufacturing and design cost of the other orthogonal polarization. The phased array incorporates beamforming ICs (BFIC) which are connected to radiating elements in 2x2 architecture. The performance of the 28-GHz phased array with high EIRP and a low-complexity PCB employing waveguide-based antennas is good and can be adequately employed for 5G applications requiring high-power at 64 dBm and wide-angle beam scanning up to positive and negative 40° in the azimuth.

Disclaimer: This work has been performed in the framework of the H2020 project WaveComBE (Grant agreement ID: 766231) co-funded by the EU. This information reflects the consortium's view, but the consortium is not liable for any use that may be made of any of the information contained therein. This deliverable has been submitted to the EU commission, but it has not been reviewed and it has not been accepted by the EU commission yet.

List of figures

Fig. 1 The 28-GHz 8x8 phased array antenna prototype based on Gap waveguide

Fig. 2 (a) shows the calibration value versus frequency, and (b) radiation pattern of the horn antenna in azimuth plane (E-plane) at 28 GHz after calibration.

Fig. 3 measured S21 for the two circuits and loss of the passive board.

Fig. 4 Computed antenna gain of the 8-slot antenna compared to the gain of the 4-slot antenna.

Fig. 5 Calibrated pattern of the antenna (a) in the azimuth plane, i.e., the E-plane and (b) in the elevation plane, i.e., the H-plane.

Fig. 6 The normalized radiation patterns.

Fig. 7 The difference in gain between two antennas in the broadside.

Fig. 8 (a) Gain of the active board and (b) EIRP of the antenna in the broadside direction as function of frequency.

Fig. 9 (a) Antenna gain and (b) EIRP at 26.5 GHz

Fig. 10 (a) Antenna gain and (b) EIRP at 27 GHz

Fig. 11 (a) Antenna gain and (b) EIRP at 27.5 GHz

Fig. 12 (a) Antenna gain and (b) EIRP at 28 GHz

Fig. 13 (a) Antenna gain and (b) EIRP at 28.5 GHz

Fig. 14 (a) Antenna gain and (b) EIRP at 29 GHz

Fig. 15 (a) Antenna gain and (b) EIRP at 29.5 GHz

Fig. 16 The angle corresponding to maximum EIRP versus frequency.

Fig. 17 (a) The maximum EIRP, and (b) the maximum gain of antenna versus LUT number.

Fig. 18 The stack-up of the 16x16 slots phased array antenna designed with a 6-layer PCB and gap waveguide-based antennas.

Fig. 19 A block diagram of RF components on the PCB.

Fig. 20 A manufactured prototype of the active 16x16 slots phased array antenna

Fig. 21 Linear subarray

Fig. 22 Active reflection coefficients for five different scanning angles

Fig. 23 Radiation pattern of co-polarized and cross-polarized components for (a) broadside and (b) scanning to -40° in the azimuth.

Fig. 24 Radiation pattern scanning with 1° resolution in azimuth

List of Acronyms and Abbreviations

2D	two dimensional
5G	5th Generation
BFIC	beamforming ICs
CMOS	Complementary metal–oxide–semiconductor
EIRP	effective isotropic radiated power
EVM	error vector magnitude
IC	integrated circuit
LO	local oscillator
MED	magneto-electric dipole
MIMO	multiple-input multiple-output
mmWave	millimeter wave
PAAM	phased array antenna module
PCB	printed circuit board
PNA	performance network analyzer
RF	radio frequency
RX	receiver
SiGe	silicon-germanium
SMA	SubMiniature version A
SPI	serial peripheral interface
TX	transmitter
UDC	frequency up/down converter
VGA	variable gain amplifier
WLCSP	wafer-level chip scale packaging

1. Introduction

The fifth generation (5G) wireless communication systems are expected to provide multiple users with Gbps peak data rates simultaneously. Moving to the millimeter-wave (mmWave) spectrum offers unprecedented unlicensed bandwidth, and therefore it has been advocated as a solution to realize this challenging vision. However, when compared to the lower frequency bands, mmWave communication suffers from more significant propagation path loss [1]. Therefore, mmWave communication links will rely on highly directive communications to deal with propagation loss [2]. To this end, a variety of directive antennas based on different transmission line technologies, such as waveguide [3], substrate integrated waveguide [4], and gap waveguide [5], have been proposed. Although these antennas allow for low-loss directive communication, the coverage area of the directive communication link is limited due to the directive beam's narrow beamwidth.

For directive communication with a large coverage area, multibeam array antennas [6] or phased array antennas [7] are required. For military and satellite communication, multibeam array and phased array antennas have traditionally been used. The main disadvantage of multibeam antennas is that their feeding networks are typically bulky and complex, making them difficult to implement in large array configurations with 2D scanning [6]. These multibeam antennas typically have 2 by 2 configuration for 2D multibeams, which is insufficient for a 5G outdoor base station [8], [9]. A minimum of 32 elements (4 x 8) is recommended to achieve high effective isotropic radiated power (EIRP) and Gb/s data links over hundreds of meters [10]. To make a larger array antennas with multibeams, 1D distributed beam is possible, but it gives less flexibility in the implementation for the base station [6], [11].

A better alternative is a phased array antenna that allows the antenna beam to be electronically scanned [7]. However, in order for phased arrays to be widely used in 5G applications, their development and manufacturing costs must be significantly reduced. Low-cost active beamformers have been developed thanks to silicon technologies (SiGe and CMOS) [10]. For millimeter wave 5G communication, numerous phased array antennas have been designed [7], [10], [12], [13]. The majority of these studies, however, have focused on the design and optimization of beamformer performance. These phased array antennas used traditional patch antennas to produce beamsteering arrays [7], [10], [12]. These patch antennas, on the other hand, usually have a narrow bandwidth (~6%) and a high cross polarization [7], [10]. A parasitic patch is required to improve the bandwidth performance of these patch antennas, but the bandwidth of the designed patch antenna is still insufficient to cover the proposed N257 mmWave band (26.5 - 29.5 GHz) for 5G communication [7], [10]. The bandwidth of these patch antennas could be increased by 25%, allowing them to cover the entire mmWave 5G band (24.25 - 29.5 GHz) with an additional impedance matching circuit over the feeding network. However, this increases the integration complexity [13].

Wideband antennas with simple feeding which cover the 5G band are therefore in high demand. The magneto-electric dipole (MED) antenna was a widely proposed antenna in the development of previous generation (3G and 4G) wireless communication systems [14]. The MED enables both the electric and magnetic dipoles to be excited at the same time, resulting in wideband performance [14], [15]. MED has recently been used in the development of a mmWave high gain fixed beam array antenna [16]. Depending on the feeding technique, most of these antennas provide a very wideband performance (>25%) [14]. Unfortunately, the size of these antennas is usually quite large (around λc , where λc is the wavelength at the center frequency) [14]. As a result, these MED antennas are not directly applicable to the design of phased array antenna

systems, due to the presence of unwanted radiating grating lobes. Thus, the MED need to be redesigned to in order to be employed as the antenna element of a phased array antenna.

In this deliverable we present two phased array antenna prototypes based on the Gap waveguide technology that have been fabricated and characterized. These are a 28-GHz 8x8 phased array with 60dBm EIRP, and a 28-GHz 16x16 phased array with 45°-slanted polarization and 65dBm EIRP, which are presented in Sections 2 and 3, respectively.

2. A 28-GHz 8x8 phased array antenna based on Gap waveguide with 60dBm EIRP

2.1 Antenna structure description

Fig. 1 shows the 28-GHz 8x8 phased array antenna prototype based on Gap waveguide.

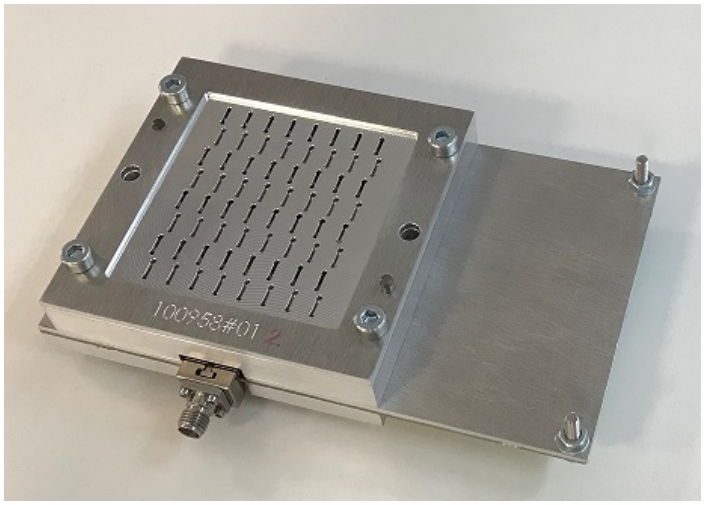

Fig. 1 The 28-GHz 8x8 phased array antenna prototype based on Gap waveguide

2.2 Passive measurements

The goal in this test is to determine the gain of the phased array antenna in the broadside direction of the antenna in the frequency band of interest. For this purpose, first it is needed to calibrate the measurement setup with a standard reference antenna. A horn antenna is used here. Then, the losses in the passive circuits which include the microstrip lines and the Wilkinson power dividers is measured. Finally, the gain of the phased array antenna (or just antenna in the following) is computed from the measurement data. In the following subsections, each step is described.

2.2.1 Setup calibration with standard horn antenna

The antenna consists of a passive circuit which is connected to a PNA by an SMA port and to antenna by transitions from PCB board to the gap waveguide. The passive circuit is consisted of a chain of seven Wilkinson power dividers that in overall create a 1 to 8 power divider. The output of this circuit is 8 signals with equal amplitude and phase and is used to feed the antenna. The antenna array with these excitation signals will have a main lobe radiating at the broadside direction.

To calibrate the measurement setup, a standard horn antenna with known gain is used. The calibration value is the difference between S21 in the broadside angle which is read with PNA and the actual gain of the antenna. This value includes approximately the effects of coaxial cables, path loss between antenna under test and gain of the other antenna and the power provided by PNA.

$$G_{cal} = G_{Standard\ horn} - S21_{Standard\ horn\ in\ broadside}$$

Fig. 2(a) shows the calibration value versus frequency. The radiation pattern of the horn antenna in azimuth plane (E-plane) at 28 GHz after adding calibration value is shown in Fig. 2 (b).

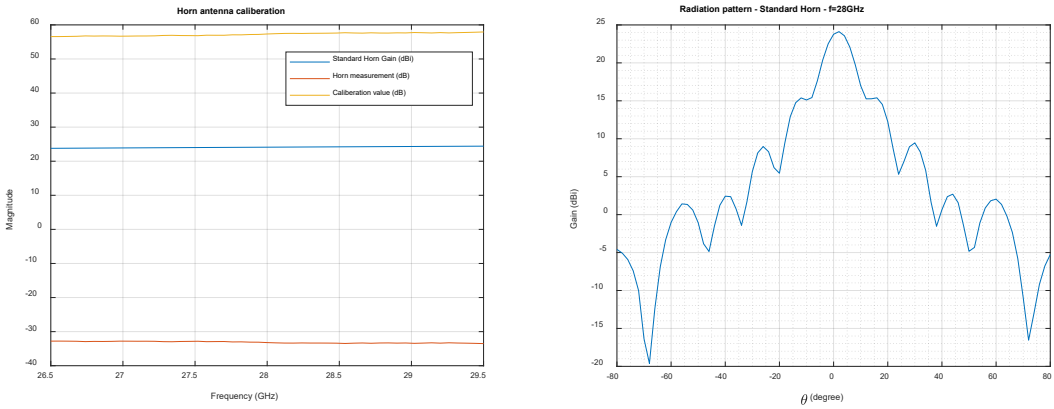

(a) (b)

Fig. 2 (a) shows the calibration value versus frequency, and (b) radiation pattern of the horn antenna in azimuth plane (E-plane) at 28 GHz after calibration.

2.2.2 Measuring loss in the passive board

We used two circuits for measuring the loss in the passive board. The first one is a 50 Ohm microstrip line with the length of 35.4 mm. The loss in the microstrip line per unit of length can be measured with this circuit. The second circuit consists of two chains of 1 to 8 Wilkinson power dividers which are placed back-to-back to each other. This circuit also has two microstrip lines which connect the back-to-back structure to the connectors and length of each line is 17.6 mm. The loss in the chain of Wilkinson power divider can be measured with this circuit.

For the loss measurements, the PNA is calibrated, and two adaptors are used to connect the extenders to the circuits' SMA ports. Thus, in the computation of passive board losses, the loss in the adaptors and SMA is considered. The loss for the adaptor and the SMA is 0.2 dB, hence $L_{connector} = -0.2\ dB$.

The loss per unit length is computed by

$$L_{ustrip} = \frac{S21_{ustrip} - 2 * L_{connector}}{35.4}\ [dB/mm].$$

The loss in the chain of 1 to 8 Wilkinson power divider is then computed as

$$L_{Wilkinson} = \frac{S21_{Wilkinson}}{2} - L_{connector} - L_{ustrip} * 17.6.$$

Finally, the loss in the passive board is obtained by the following equation

$$L_{passive} = L_{Wilkinson} + L_{ustrip} * 39.8 + L_{connector}.$$

The length of the microstrip line in the passive board is 39.8 mm.

Fig. 3 shows the measured S21 for the two circuits and the loss of the passive board which is computed with above equation.

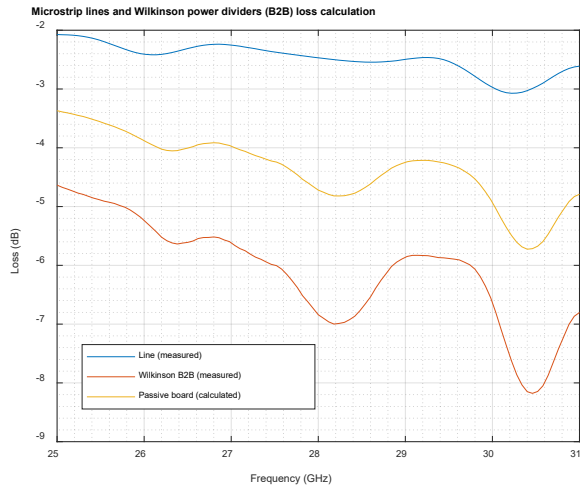

Fig. 3 measured S21 for the two circuits and loss of the passive board

2.2.3 Computing the antenna based on the passive measurement setup

The next step is to compute the antenna gain obtained from the measurement setup. The gain of the antenna is computed by using the calibration value and loss in the passive board.

$$G_{antenna} = S21_{antenna\ in\ broadside} + G_{cal} - L_{passive}$$

The computed antenna gain is compared to the gain of 4-slot antenna, which has also been computed employing the passive board, which results are shown in Fig. 4. The calibrated pattern of the antenna in the azimuth (E-plane) and the elevation (H-plane) planes are depicted in Fig. 5 (a) and (b), respectively. Before making any comparison, we must make sure that the antenna has its maximum gain in the horizontal plane. Therefore, pattern of the antenna is measured in both the elevation and the azimuth planes at 28 GHz. The normalized radiation patterns are shown in Fig. 6. The difference in gain between two antennas in the broadside is shown in the Fig. 7.

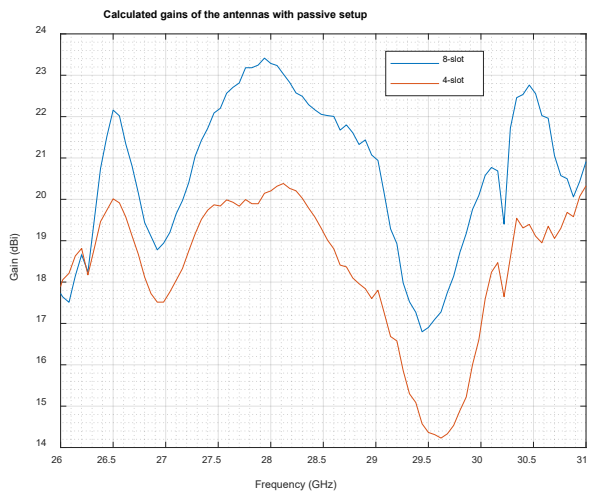

Fig. 4 Computed antenna gain of the 8-slot antenna compared to the gain of the 4-slot antenna

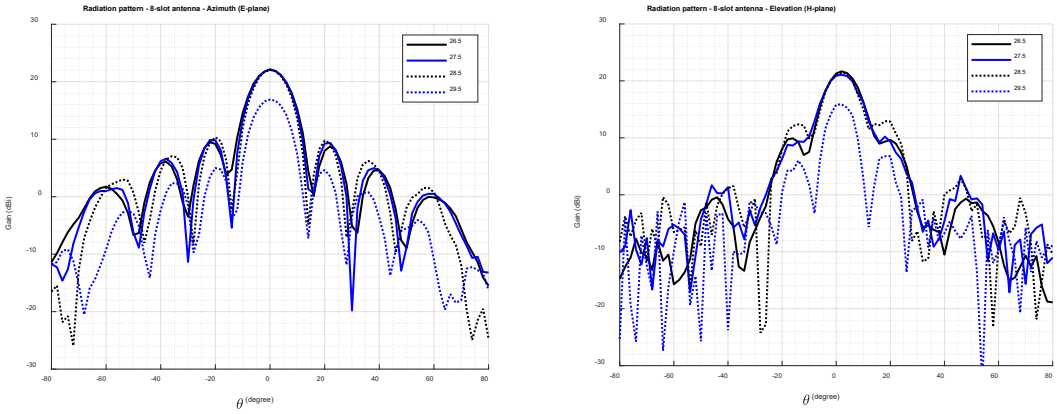

(a) (b)

Fig. 5 Calibrated pattern of the antenna (a) in the azimuth plane, i.e., the E-plane and (b) in the elevation plane, i.e., the H-plane

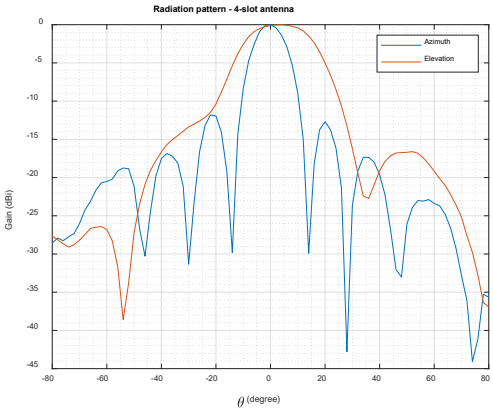

Fig. 6 The normalized radiation patterns.

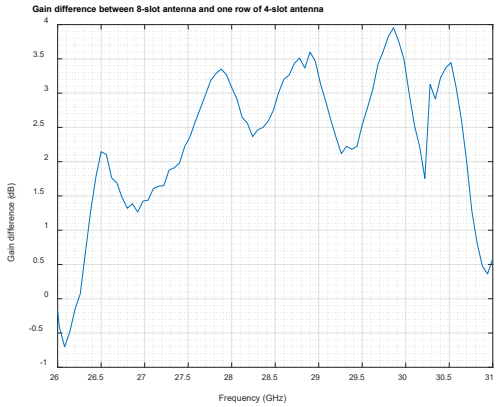

Fig. 7 The difference in gain between two antennas in the broadside

2.3 Active Measurements

The goal of this test was to evaluate the steering capability of the antenna in the main lobe. A total of 21 sets of steering weights (phase and amplitude) are defined for the antenna array and each set is measured separately. These 21 sets of phase and amplitudes gave us the possibility to steer the beam in the E-plane of the antenna. The gain of the active circuit is computed by using the results of the previous section. Since we know the gain of the antenna in the broadside angle (direction), we first compute the gain of the active board with the results of measurement at this steering angle. Then, we can compute the antenna gain in the steering angles other than broadside.

2.3.1 Measuring gain of the active board

In this part the gain of the active board is computed. We measured the radiation pattern of the antenna in broadside angle and then used the equation below to compute the gain of the active board.

$$G_{active\ board} = S21_{antenna\ in\ broadside} + G_{cal} - L_{active} - G_{antenna}$$

$$EIRP_{broadside} = S21_{antenna\ in\ broadside} + G_{cal}$$

In the computations, we considered $L_{active} \approx L_{passive}$. The gain of the active board is shown in Fig. 8. The gain of the active antenna (EIRP) in broadside over frequency domain, which includes loss and gains of antenna and active board, is shown in Figure 10.

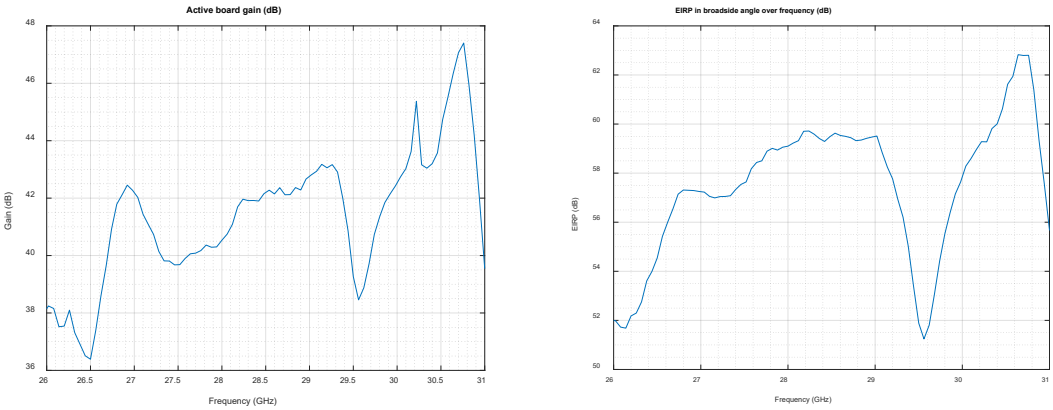

Fig. 8 (a) Gain of the active board and (b) EIRP of the antenna in the broadside direction as function of frequency.

2.3.2 Computing the radiation gain pattern at different tilting angles

In this section, the radiation in the azimuth plane (E-plane of antenna) is presented for the considered 21 steering angles. The gain of the other 20 states (LUTs) of the antenna, i.e., other than broadside angle, which was computed in last section, are computed using these equations

$$G_{antenna\ other\ than\ broadside} = S21_{antenna\ other\ than\ broadside} + G_{cal} - L_{active} - G_{active\ board},$$

$$EIRP_{other\ than\ broadside} = S21_{active\ antenna\ other\ than\ broadside} + G_{cal}.$$

In order to compute the antenna gain, we assumed that the gain of the active board does not change when varying the steering angle of the antenna. In other words, we used the gain of the active board obtained above for all LUTs, which is only valid for broadside angle. But the computed antenna gain in next figures are valid with ±1 dB error due to change of the gain in active board. In Fig. 9 to 15, the antenna gain (plots with caption (a)) and the radiation patterns of EIRP (plots with caption (b)) are shown for 21 LUT states at 7 frequencies. The angle corresponding to maximum EIRP versus frequency are shown in Fig. 16. The maximum EIRP and the maximum gain of antenna versus LUT number are shown in Fig. 17 (a) and (b), respectively.

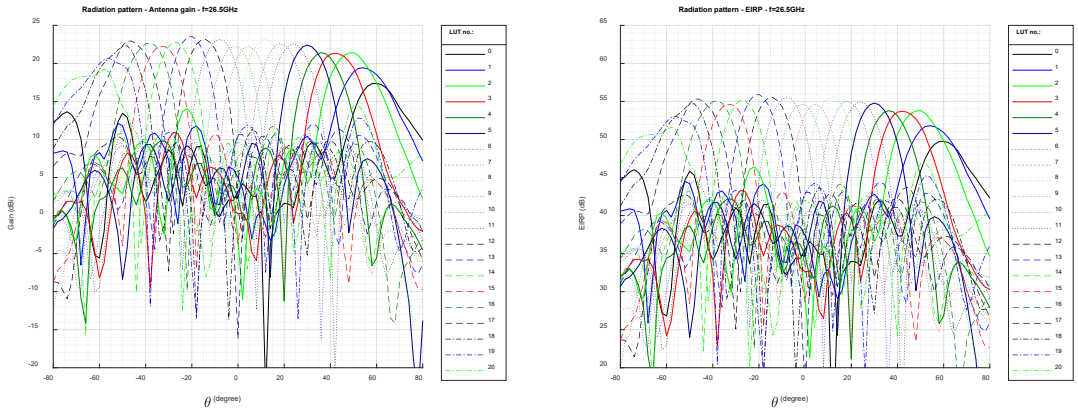

(a) (b)

Fig. 9 (a) Antenna gain and (b) EIRP at 26.5 GHz

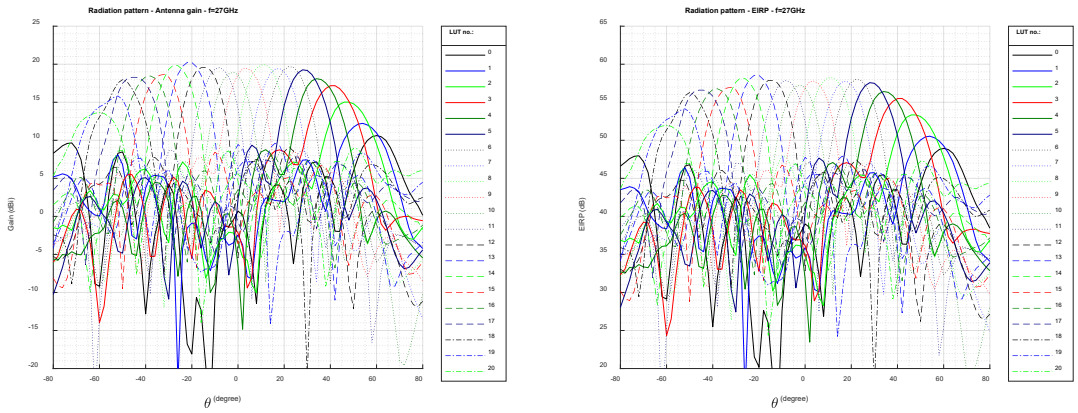

(a) (b)

Fig. 10 (a) Antenna gain and (b) EIRP at 27 GHz

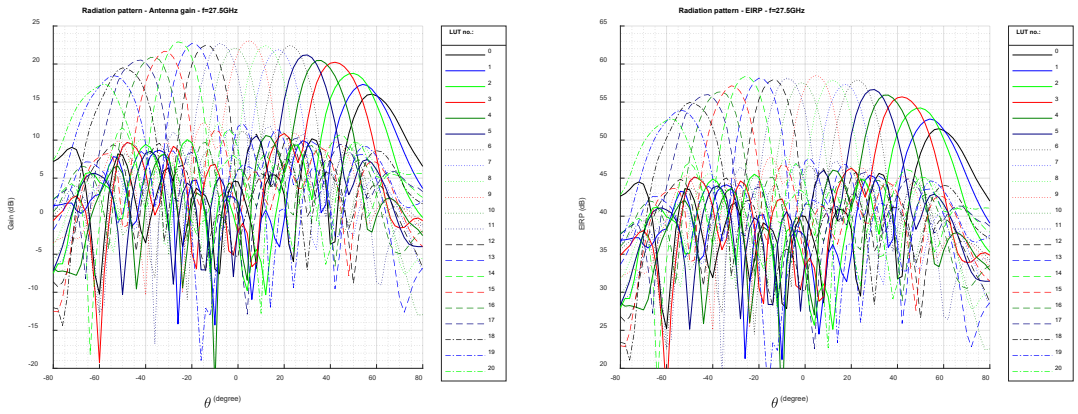

(a) (b)

Fig. 11 (a) Antenna gain and (b) EIRP at 27.5 GHz

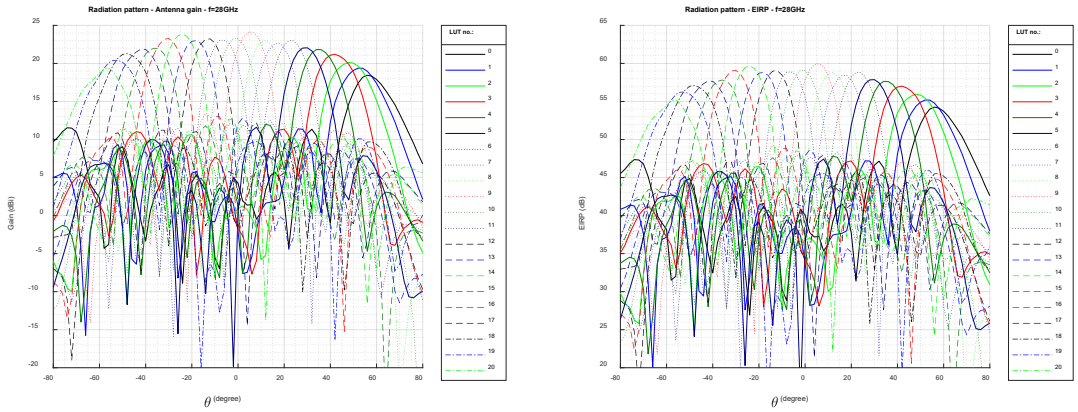

(a) (b)

Fig. 12 (a) Antenna gain and (b) EIRP at 28 GHz

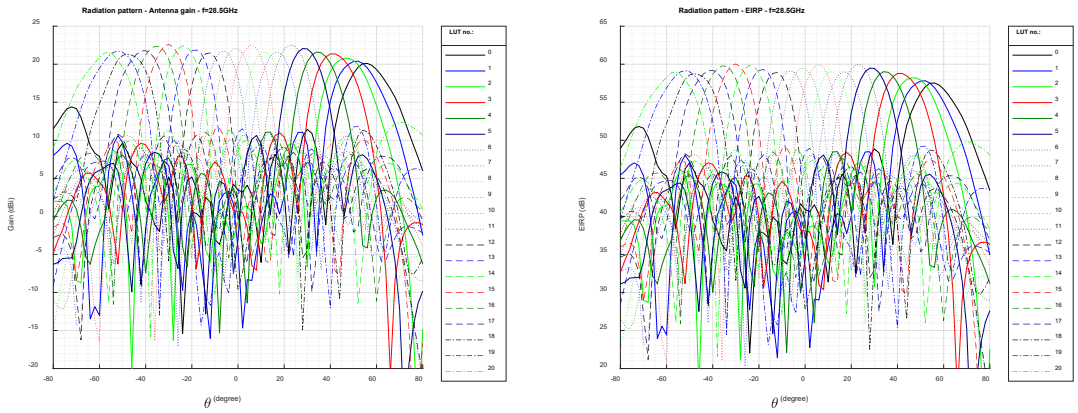

(a) (b)

Fig. 13 (a) Antenna gain and (b) EIRP at 28.5 GHz

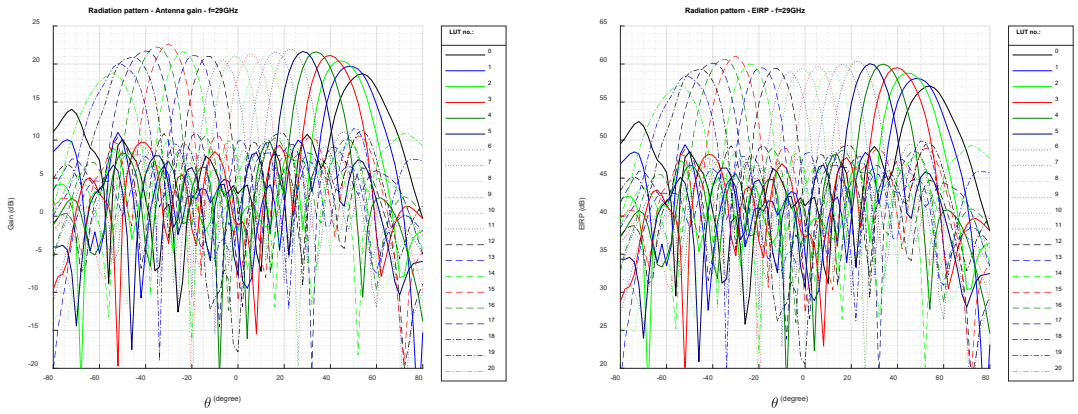

(a) (b)

Fig. 14 (a) Antenna gain and (b) EIRP at 29 GHz

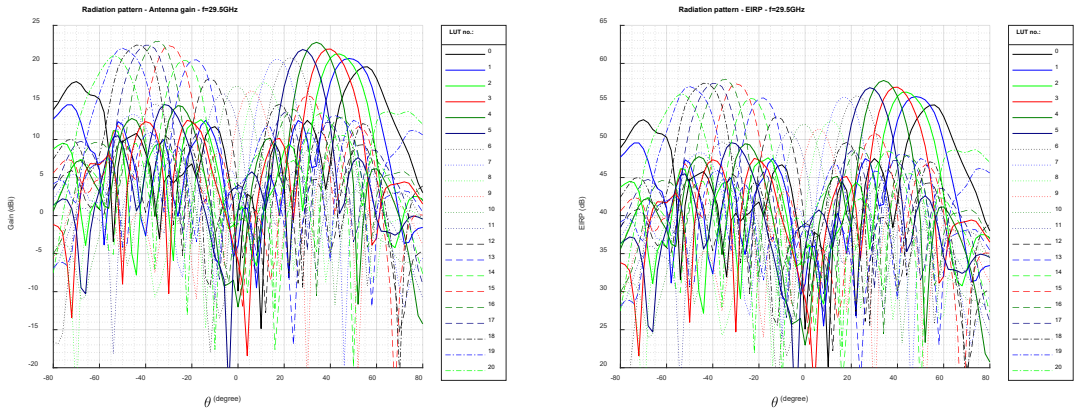

(a) (b)

Fig. 15 (a) Antenna gain and (b) EIRP at 29.5 GHz

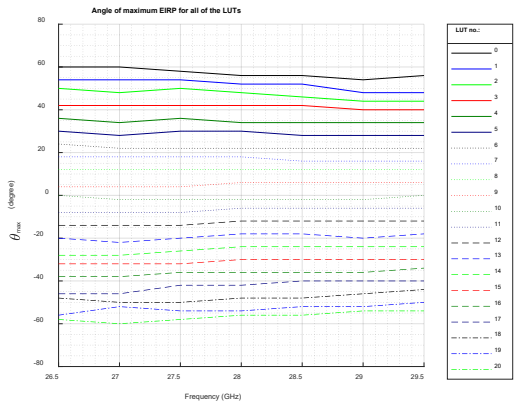

Fig. 16 The angle corresponding to maximum EIRP versus frequency.

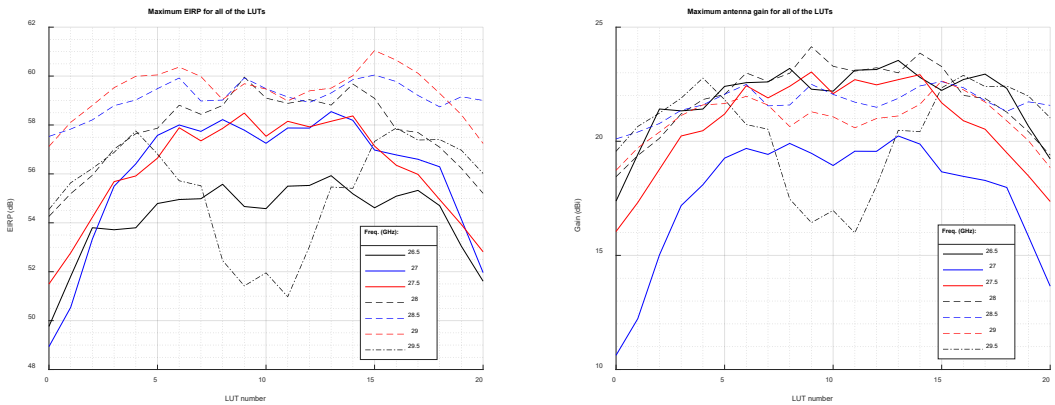

(a) (b)

Fig. 17 (a) The maximum EIRP, and (b) the maximum gain of antenna versus LUT number.

3. A 28-GHz 16x16 phased array based on Gap waveguide with 45°-slanted polarization and 65dBm EIRP.

In this section we present the design and characterization of a manufactured phased array antenna where antenna elements are not implemented on PCB. Gap waveguide-based antennas have great integration flexibility with PCB as the carrier of the active components and suitable for mmWave frequencies. So, the PCB can be manufactured with minimum number of layers, based on biasing and control signal requirements. We employ the basic idea proposed in [24],[25], i.e., a microstrip probe transition from microstrip to waveguide and then to ridge gap waveguide is designed.

The antenna unit element proposed here is a subarray of four slanted slots over a Gap waveguide line. Employing subarray in the design of antenna elements, helped to have many radiating elements while keeping the number of transmitting and receiving modules low, so less hardware is required. This is important for low-rise urban, suburban, and rural areas, where the vertical spread of users is low and coverage in that axis can be decreased. Subarraying helps with keeping the antenna area large which is necessary for improving uplink cell-edge coverage while minimizing the number of radio chains [26]. The subarray architecture for a fixed EIRP reduces power consumption. Hence, subarraying allows for lower power consumption and even less cost. But the expense to be paid for these advantages is the reduced scanning range in one of the principal scanning planes, which in this article is elevation.

The presented phased array employs a subarray of four slots with 45° slant polarization in resonant center-fed waveguide. The 45°slant polarization reduces the manufacturing and design cost of the other orthogonal polarization [27]. Therefore, two orthogonal polarizations with totally symmetric structures can be achieved. Employing ±45° slant polarizations provide a more symmetrical propagation characteristics in mobile communication systems, than horizontal/vertical polarization [28].

In this section, we present our approach to tackle the challenge of designing a 28-GHz phased array with high EIRP and a low-complexity PCB employing waveguide-based antennas.

3.1 Phased Array Design

The 16x16 slots phased array is designed with a 6-layer PCB and gap waveguide-based antennas. The stack-up of the antenna is shown in Fig. 18. The antenna layers (slot and distribution) are placed at top of the PCB. A block diagram of RF components on the PCB is shown in Fig. 19. The array employs four mmWave frequency up/down converter (UDC) ICs produced in 300mm Silicon CMOS process, with x4 local oscillator (LO) multiplier [29]. Each UDC supports a quarter of array, and all quarters have similar structures. UDCs are connected to a separate LO, TX and RX connectors with 50 Ohm striplines, meaning that each UDC can function independent of how other UDCs are configured. So, it is possible to produce four beams at the same time with this design. In this article, the LO frequency is set to 6GHz and the IF band (both for RX and TX) is set to 2.5-5.5GHz.

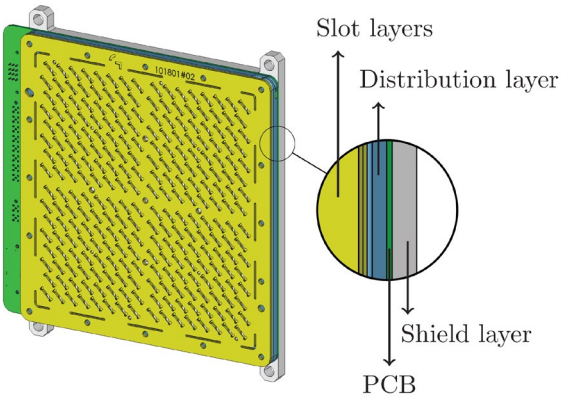

Fig. 18 The stack-up of the 16x16 slots phased array antenna designed with a 6-layer PCB and gap waveguide-based antennas.

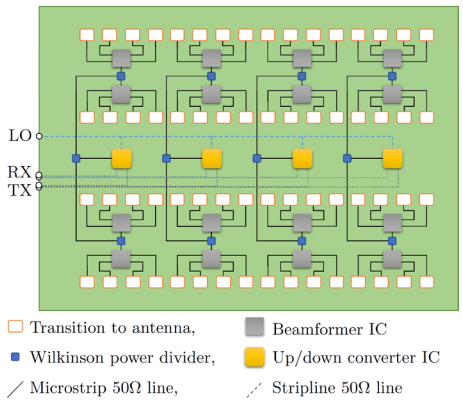

Fig.19 A block diagram of RF components on the PCB.

The phased array incorporates beamforming ICs (BFIC) which are connected to radiating elements in 2x2 architecture, as shown in Fig. 19. BFICs have four bidirectional channels and are digitally controlled via a high-speed serial peripheral interface (SPI) bus [30]. Each channel employs a TX chain and a RX chain, which each chain includes a high-resolution phase shifter and variable gain amplifier (VGA). Gain control of VGAs in TX and RX chains are 25dB and 30.5dB, respectively. Each channel's transmit chain P1dB of is 19dBm. The SPI interface controls all device functions. This BFIC uses a wafer-level chip scale packaging (WLCSP) with compact dimensions of 4.39x3.59x0.5mm^3.

The PCB stackup incorporates 6 layers of metals. The top metal layer (M1) hosts the UDCs, BFICs, wilkinson power dividers and all 50 Ohm microstrip routing lines. Layer M4 is used for the main trace of striplines. Layers M2 and M6 are used for grounding purposes of IF and RF frequency signals. Each channel of BFIC is connected to a transition from microstrip to double ridge waveguide. A microstrip-probe with back-short alongside with vias on the PCB, create the transition to waveguide. The PCB is based on RO4350B (ε_r=3.66$, tand=0.0037) and RO4450F (ε_r =3.7, tand=0.004) as core and prepreg substrates, respectively.

A manufactured prototype of the phased array antenna is shown in Fig. 20.

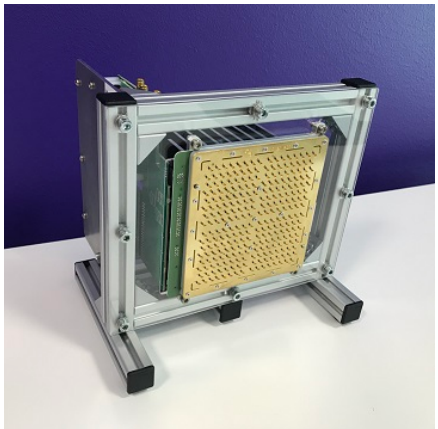

Fig. 20 A manufactured prototype of the active 16x16 slots phased array antenna

3.1 Antenna Design and Measurements

The proposed antenna employs a linear subarray of four slots as the antenna element as shown in Fig. 21. The linear subarray is oriented in elevation direction and is fed from the middle through a microstrip to gap waveguide transition. Although having a subarray decreases the beamwidth in elevation direction, and consequently limits the scanning rage of the phased array antenna, but it increases the gain per BFIC channel. Higher gain per element is beneficial especially in uplink when the output power of the user is very low.

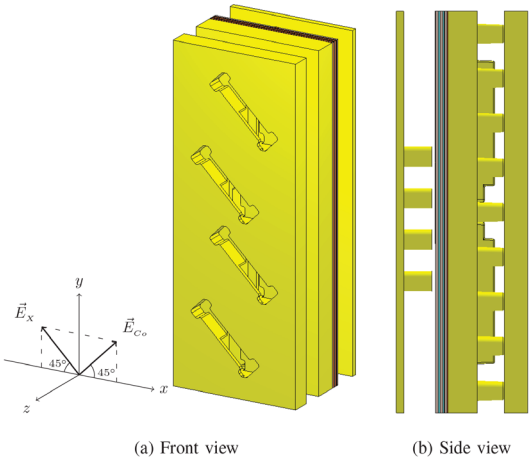

(a) Front view (b) Side view

Fig. 21 Linear subarray

Employing 45°-slanted slots in the subarray creates a great opportunity of having the other orthogonal polarization with no additional design. This approach gives us two orthogonal polarizations with very similar performance, due to symmetrical structure. Traditionally, two orthogonal polarizations are created vertically and horizontally. The drawback of the second approach, no matter the antenna element is designed based on substrate or waveguide, is different performance of the polarizations, e.g., gain, bandwidth, scanning range, cross-polarization level, etc. [22], [23], [31].

The antenna element is composed of 4 series 45°-slanted center-fed slots. These slots are over a gap waveguide transmission line, and the excitation of slots are like those which previously presented [27]. In the design of the transmission line, it is essential to make sure that the pins' stopband covers the working bandwidth of the phased array to minimize the leakage between subarrays. Another important consideration in the design of gap waveguide transmission line is to check propagating mode characteristics. Indeed, with only one pin on two sides of the ridge, a single mode band of 21-53 GHz is achieved. This quasi-TEM mode which covers the working bandwidth of phased array, is employed to excite the slots. Each subarray is excited through a vertical microstrip-probe with backshort. The backshort is realized on the shield layer, and its walls are built employing cylindrical pins, which create a stopband of 25-57GHz.

Subarray performance is investigated by two approaches. First, the subarray is simulated in unitcell structure meaning that the boundary conditions in the sides are set to be periodic. Another approach in the simulation of the array element, is according to the position of the element in the antenna array. Basically, the position of the element in the array plays a role in the radiation properties of that element, which are referred to embedded results. Elements of the antenna array are simulated one by one, while other elements are perfectly matched.

After the subarray design, the so-called active reflection coefficients of the array are calculated, which are shown in Fig. 22 for five different scanning angles. Due to similarity, only results of a quarter of antenna array elements are shown here. The antenna shows good matching for all scanning angles up to close ±60°in azimuth plane (lower than -10dB).

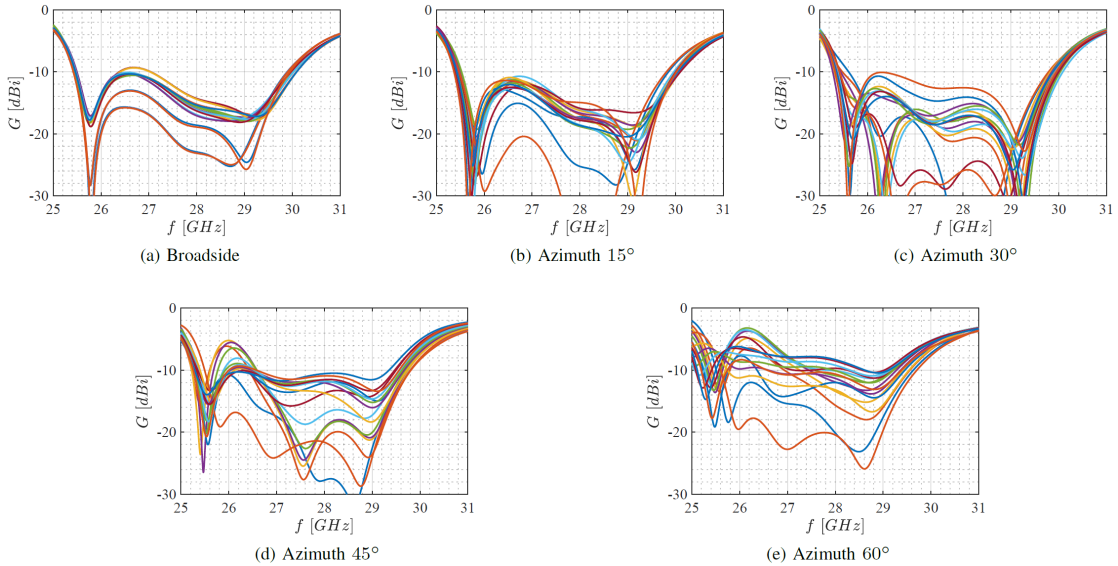

Fig. 22 Active reflection coefficients for five different scanning angles

3.2 Calibration and Pattern Measurement of the PAAM

To achieve the desired performance from the phased array module, there is a need for calibration. Even though the RF-lines have equal length, there will be unavoidable differences between channels due to manufacturing, assembly, passive components, and differences between the BFICs. If the phase difference between channels is too great, the resulting farfield pattern may display large side lobes, beam pointing in an undesired direction and consequently a lowering of main lobe gain reducing the overall performance. A random gain variation across channels may influence the EVM negatively, but this also depends on how close to backoff the module is operated and how large the variation is [32]. For this work, only channel phase calibration has been performed and no channel gain calibration is considered. However, due to unequal length in the IF-feed network for the four UDCs, a calibration of the UDC-gain levels was performed to have a more even gain distribution across the array when combining all 64 channels.

A study of the simulated performance deviation arising from a random element excitation error in phase and amplitude. The element amplitude error is varied with ±3 dB, and the phase error is varied with ±20°. The resulting error in main lobe gain, side lobe level and pointing error for broadside and 45° azimuth scan for 100 iterations with random errors was evaluated. The observed main lobe gain variation was less than ±1 dB for both scan angles, and the pointing error was relatively unaffected by the random errors applied. The side lobe level however can vary ±2 dB depending on excitation, showing that calibration is needed if one wishes to keep side lobe level close to nominal value.

After calibration, the antenna's performance is tested in an anechoic chamber in both TX and RX mode. The gain and side lobe level of the antenna at different frequencies and scanning angles were evaluate. It was obtained that the antenna in TX mode has 64dBm EIRP at P1dB. Two examples of radiation pattern of co-polarized and cross-polarized components of radiation

pattern are shown in Fig. 34a and 14b, for broadside and scanning to azimuth -40° respectively. The antenna has shown a fine scanning resolution. Fig. 24 shows the radiation pattern scanning with 1° resolution (1° is the limit we had during the measurement process).

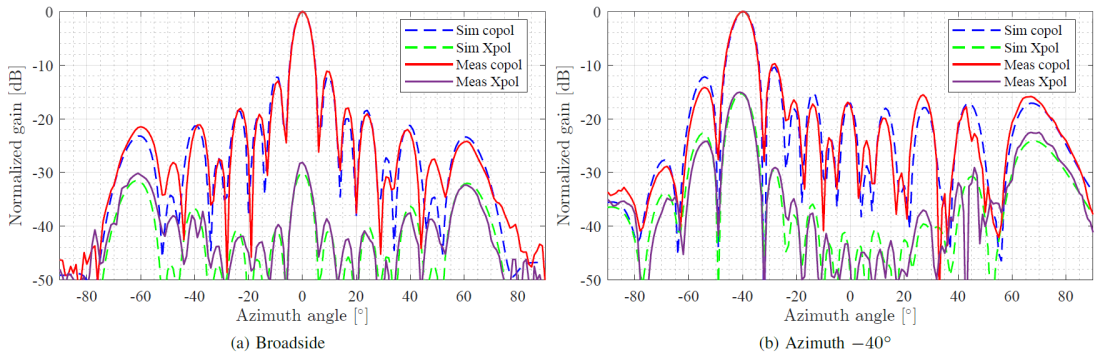

Fig. 23 Radiation pattern of co-polarized and cross-polarized components for (a) broadside and (b) scanning to -40° in the azimuth.

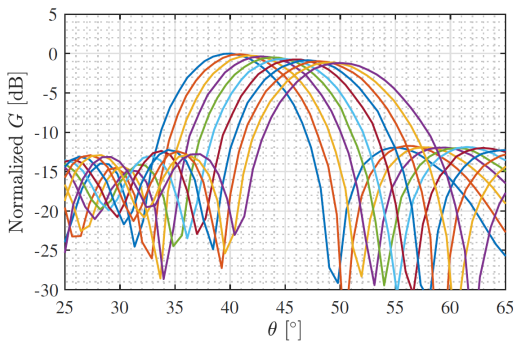

Fig. 24 Radiation pattern scanning with 1° resolution in azimuth

4. Conclusions

Measured performance of two 5G phased array antenna designs have been presented. The two phased array antenna prototypes are based on the Gap waveguide technology and have been fabricated and characterized. These are a 28-GHz 8x8 phased array with 60dBm EIRP, and a 28-GHz 16x16 phased array with 45°-slanted polarization and 65dBm EIRP

The first 8x 8 antenna was compared to the 4x8 subarray (or 4-slot) array antenna configuration based on the same design. The broadside gain of the antennas was computed from the measurement data. Also, measurement results of the EIRP when beam of antenna is scanned in the E-plane. The antenna was expected to have 23 dBi gain on average in the frequency band from 26.5 - 29.5 GHz. However, this was not fully achieved for the 8-slot antenna. Compared to the measured gain of the 4-slot antenna a 3 dB difference between the gains the two antenna realizations was expected. The difference in the lower frequency band lower than expected, on the other hand at higher frequencies, namely 27.5 to 29.5 GHz, we can roughly see 3 dB gain difference on average which is good. Moreover, the S11 of the antenna structure with the passive board has very poor response (results will be added later). The high return loss reduces the gain of the antenna. Also, resonances where observed at 29.5 GHz in both the 4-slot and 8-slot broadside antenna gain responses versus frequency. At that frequency, significant loss of gain around 6 dB is observed, which also exists in the EIRP measurement results in broadside radiation. The origin of the resonance should not come from the antenna array layers

(distribution and slot layers) or the active, or the passive, boards. Hence, this leaves us with the probable cause to stem from either the transitions or shielding layer with pin structure. In summary, the antenna has from 1 - 1.5 dB less gain than expected, explained by poor S11 response causes the reduction of antenna gain in all frequencies, and a resonance in the antenna gain response is present at 29.5 GHz caused problems in transitions or shielding layer with pin structure.

An updated antenna design with optimize antenna performance will be presented later in future versions of the report. A journal paper contribution will be submitted based on the updated results: Alireza Bagheri, Carlo Bencivenni, Magnus Gustafsson, Andrés Alayón Glazunov, A 28-GHz 8x8 phased array based on gap waveguide with 60 dBm EIRP, IEEE Antenna and Wireless Propagation Letters (to be submitted 2021)

The second array employs a linear subarray of four 45°- slant polarized slots as the antenna element. The 45°-slant polarization reduces the manufacturing and design cost of the other orthogonal polarization. The phased array incorporates beamforming ICs (BFIC) which are connected to radiating elements in 2x2 architecture. The performance of the 28-GHz phased array with high EIRP and a low-complexity PCB employing waveguide-based antennas is good and can be adequately employed for 5G applications requiring high-power at 64 dBm and wide-angle beam scanning up to positive and negative 40° in the azimuth.

Based on the presented results two papers will be submitted to topical journals: Alireza Bagheri, Hanna Karlsson, Carlo Bencivenni, Magnus Gustafsson, Thomas Emanuelsson, Marcus Hasselblad, Andrés Alayón Glazunov, A 28-GHz 16x16 phased array based on gap waveguide with 45°-slanted polarization and 65 dBm EIRP, IEEE Transactions on Microwave Theory and Techniques (to be submitted 2021), Alireza Bagheri, Hanna Karlsson, Jose-Ramon Perez, Parastoo Taghikhani, Thomas Emanuelsson, Christian Fager, Carlo Bencivenni, Andrés Alayón Glazunov, OTA characterization of a phased array at mmWave to verify 5G application, IEEE Wireless Communication Magazine – Special Issue on Antenna Systems for 5G and Beyond. 2021. (to be submitted 2021)

In addition, a couple of other phased array antennas based on the MED technology are currently being manufactured and characterized. The design and measurements will be submitted to topical journals as listed below.

A. List of Publications (published and in preparation)

1. W.Y.Yong. T.Emanuelsson and A.A.Glazunov. 5G Wideband Magneto-Electric Dipole Antenna Fed by a Single-Layer Corporate-Feed Network based on Ridge Gap Waveguide. 2020 14th European Conference on Antennas and Propagation (EuCAP 2020). Pp.1 – 4. 2020.
2. W.Y.Yong. T.Emanuelsson and A.A.Glazunov. 4× 4 Magneto-Electric Dipole Array with Single-Layer Corporate-Feed Ridge Gap Waveguide for mmWave Applications. nternational Symposium on Antennas and Propagation, ISAP 2020. Pp. 1 – 2. 2021.
3. Wai Yan Yong and Andrés Alayón Glazunov, “High Gain, Wideband Grid Array Antenna for 28 GHz 5G Base Station,” *European Conference on Antenna and Propagation (EuCAP)* 2019, Krakow, Poland.
4. Alireza Bagheri, Carlo Bencivenni, Andrés Alayón Glazunov, “mmWave Antenna Array based on Gapwaves Waveguide Technology for 5G Applications,” *International Conference on Electromagnetics in Advanced Applications (ICEAA) 2019*, Granada, Spain.

5. Wai Yan Yong, Abolfalz Haddadi, Thomas Emanuelsson and Andrés Alayón Glazunov. Wideband 2 by 2 Integrated Antenna Array for N257 mmWave 5G Communication. IET Electronics Letters. (to be submitted 2021)
6. Wai Yan Yong, Abolfalz Haddadi, Thomas Emanuelsson and Andrés Alayón Glazunov. Design and Characterization of the 8 by 8 Phased Array Antenna based on Magneto-Electric Dipole (MED) for 5G mmWave Outdoor Base Station. IEEE Wireless Communication Magazine – Special Issue on Antenna Systems for 5G and Beyond. 2021. (to be submitted 2021)
7. Alireza Bagheri, Carlo Bencivenni, Magnus Gustafsson, Andrés Alayón Glazunov, A 28-GHz 8x8 phased array based on gap waveguide with 60 dBm EIRP, IEEE Antenna and Wireless Propagation Letters (to be submitted 2021)
8. Alireza Bagheri, Hanna Karlsson, Carlo Bencivenni, Magnus Gustafsson, Thomas Emanuelsson, Marcus Hasselblad, Andrés Alayón Glazunov, A 28-GHz 16x16 phased array based on gap waveguide with 45°-slanted polarization and 65 dBm EIRP, IEEE Transactions on Microwave Theory and Techniques (to be submitted 2021)
9. Alireza Bagheri, Hanna Karlsson, Jose-Ramon Perez, Parastoo Taghikhani, Thomas Emanuelsson, Christian Fager, Carlo Bencivenni, Andrés Alayón Glazunov, OTA characterization of a phased array at mmWave to verify 5G application, IEEE Wireless Communication Magazine – Special Issue on Antenna Systems for 5G and Beyond. 2021. (to be submitted 2021)

References

[1] Rappaport, T.S., Sun, S., Mayzus, R., Zhao, H., Azar, Y., Wang, K., Wong, G.N., Schulz, J.K., Samimi, M. and Gutierrez, F., " Millimeter wave mobile communications for 5G cellular: It will work!". IEEE Access,no. 1, pp.335-349. 2013.

[2] J. Zhang, X. Ge, Q. Li, M. Guizani, and Y. Zhang, "5G millimeter-wave antenna array: design and challenges," IEEE Wireless Communications, vol. 24, no. 2, pp. 106–112, 2017.

[3] Y. Miura, Y. Shibuya, J. Hirokawa, G. Yoshida, and M. Ando, "Double layer full-corporate feed hollow- waveguide slot array antenna in the 60-GHz band," IEEE Trans. Antennas Propag., vol. 59, no. 8, pp. 2844–2851, Aug. 2011.

[4] C.-M. Liu, S.-Q. Xiao, and K. Wu, "Wideband slot antenna backed by cylindrical substrate-integrated waveguide cavity," IEEE Transactions on Antennas and Propagation, vol. 67, no. 3, pp. 1509–1518, 2019.

[5] A. Vosoogh, P.-S. Kildal, and V. Vassilev, "Wideband and high-gain corporate-fed gap waveguide slot array antenna with ETSI class II radiation pattern in V-band," IEEE Trans. Antennas Propag., vol. 65, no. 4,pp. 1823–1831, Apr. 2017.

[6] W.Hong et.al., "Multibeam antenna technologies for 5G wireless communications." IEEE Trans. Antennas Propag, vol.65, no.12, pp.6231-6249.2017.

[7] K.Kibaroglu, M.Sayginer, T.Phelps, and G.M. Rebeiz, "A 64-element 28-GHz phased-array transceiver with 52-dBm EIRP and 8–12-Gb/s 5G link at 300 meters without any calibration." IEEE Trans. on Microwave Theory and Techniques, vol. 66, no. 12, pp.5796-5811.2018.

[8] Li, Y. and Luk, K.M. "60-GHz dual-polarized two-dimensional switch-beam wideband antenna array of aperture-coupled magneto-electric dipoles." IEEE Trans. on Antennas and Propagation, vol.64 , no.2, pp.554-563.2015.

[9] M.M.M.Ali,. and A.R.Sebak " 2-D scanning magnetoelectric dipole antenna array fed by RGW butler matrix," IEEE Trans. on Antennas and Propagation vol. 66, no.11, pp.6313-6321. 2018.

[10] K.Kibaroglu, M.Sayginer and G.M.Rebeiz. "A Low-Cost Scalable 32-Element 28-GHz Phased Array Transceiver for 5G Communication Links Based on a 2×2 Beamformer Flip-Chip Unit Cell.", IEEE Journal of Solid-State Circuits, vol.53, no.5. pp.1260 – 1274. 2018.

[11] K.Tekkouk et.al. Multibeam SIW slotted waveguide antenna system fed by a compact dual-layer Rotman lens." IEEE Transactions on Antennas and Propagation. No. 64, vol.2. pp.504 – 514. 2015.

[12] J. Pang et al., "A 28-GHz CMOS Phased-Array Transceiver Based on LO Phase-Shifting Architecture With Gain Invariant Phase Tuning for 5G New Radio," in IEEE Journal of Solid-State Circuits, vol. 54, no. 5, pp. 1228-1242, May 2019.

[13] Y.Yin, et al. "Wideband 23.5–29.5-GHz Phased Arrays for Multistandard 5G Applications and Carrier Aggregation." IEEE Transactions on Microwave Theory and Techniques Vol.69.No.1. 235-247.2020.

[14] K.M.Luk, , and B. Wu. "The magnetoelectric dipole—A wideband antenna for base stations in mobile communications." Proceedings of the IEEE. Vol. 100.No.7. pp. 2297-2307.2012.

[15] L.Ge, andK.M. Luk. A low-profile magneto-electric dipole antenna. IEEE Transactions on Antennas and Propagation, No.60, vol.4, 1684-1689. 2012

[16] J.Sun, A.Li, and K-M. Luk. "A High-Gain Millimeter-Wave Magnetoelectric Dipole Array With Packaged Microstrip Line Feed Network." IEEE Antennas and Wireless Propagation Letters. Vol.19.No.10 pp.1669-1673.2020.

[17] J.Y.Lee et.al. Broadband and Wide-Angle Scanning Capability in Low-Coupled mm-Wave Phased-Arrays Incorporating ILA with HIS Fabricated on FR-4 PCB. IEEE Trans. On Vehicular Technology. Vol1. No.1. pp. 1-1. 2021. (In Press)

[18] P.S.Kildal,. Foundations of antenna engineering: a unified approach for line-of-sight and multipath. Artech House, 2015.

[19] M.H.Novak, ., F.A.Miranda, and J.L. Volakis. "Ultra-wideband phased array for millimeter-wave ISM and 5G bands, realized in PCB." IEEE Transactions on Antennas and Propagation. Vol. 66. No. 12.pp 6930-6938. 2018.

[20] S.M.Moghaddam, J.Yang and A.U.Zaman. Fully-Planar Ultrawideband Tightly-Coupled Array (FPU-TCA) With Integrated Feed for Wide-Scanning Millimeter-Wave Applications. IEEE Transactions on Antennas and Propagation. Vol.68. No.9. pp. 6591 – 6601. 2020.

[21] T.R.Camelon, and G.V. Eleftheriades. "Analysis and characterization of a wide-angle impedance matching metasurface for dipole phased arrays." IEEE Transactions on Antennas and Propagation. Vol. 63.No.9.pp. 3928-3938.2015.

[22] J. Pang, R. Wu, Y. Wang, M. Dome, H. Kato, H. Huang, A. T.Narayanan, H. Liu, B. Liu, T. Nakamura,et al., "A 28-ghz cmosphased-array transceiver based on lo phase-shifting architecture withgain invariant phase tuning for 5g new radio,"IEEE Journal of Solid-State Circuits, vol. 54, no. 5, pp. 1228–1242, 2019.

[23] A. Nafe, M. Sayginer, K. Kibaroglu, and G. M. Rebeiz, “2×64-element dual-polarized dual-beam single-aperture 28-ghz phased arraywith 2×30 gb/s links for 5g polarization mimo,”IEEE Transactions onMicrowave Theory and Techniques, vol. 68, no. 9, pp. 3872–3884, 2020.

[24] Y.-C. Shih, T.-N. Ton, and L. Q. Bui, “Waveguide-to-microstrip transi-tions for millimeter-wave applications,” in1988., IEEE MTT-S Interna-tional Microwave Symposium Digest, pp. 473–475, IEEE, 1988.

[25] Y.-C. Leong and S. Weinreb, “Full band waveguide-to-microstrip probetransitions,” in1999 IEEE MTT-S International Microwave SymposiumDigest (Cat. No. 99CH36282), vol. 4, pp. 1435–1438, IEEE, 1999.

[26] P. von Butovitsch, D. Astely, C. Friberg, A. Furusk¨ar, B. G¨oransson,B. Hogan, J. Karlsson, and E. Larsson, “Advanced antenna systems for5g networks,”Ericsson White Paper, 2018.

[27] A. Bagheri, J. Petersson, A. Haddadi, and A. A. Glazunov, “A±45°dual-polarized antenna for 5g mmwave applications based on gapwaveguide technology,” in2019 International Symposium on Antennas and Propagation (ISAP), pp. 1–3, IEEE, 2019.

[28] B. Lindmark and M. Nilsson, “On the available diversity gain fromdifferent dual-polarized antennas,”IEEE Journal on Selected Areas inCommunications, vol. 19, no. 2, pp. 287–294, 2001.

[29] AWMF-0153,26.5-29.5 GHz Tx/Rx Up and Down Converter IFIC.Anokiwave.

[30] MMW9002KC,26.5-29.5 GHz 4-Channel Analog Beamforming Inte-grated Circuit. NXP Semiconductors.

[31] U. Kodak, B. Rupakula, S. Zihir, and G. M. Rebeiz, “60-ghz 64-and 256-element dual-polarized dual-beam wafer-scale phased-array transceiverswith reticle-to-reticle stitching,”IEEE Transactions on Microwave The-ory and Techniques, vol. 68, no. 7, pp. 2745–2767, 2020.

[32] S. Yin, Yusheng an Zihir, T. Kanar, Q. Ma, H. Chung, L. Gao, and G. M.Rebeiz, “A 37–42-ghz 8 × 8 phased-array with 48–51-dbm eirp, 64–qam30-gb/s data rates, and evm analysis versus channel rms errors,”IEEETransactions on Microwave Theory and Techniques, vol. 68, no. 11,pp. 4753–4764, 2020.